

# Cytochrome P450-Catalyzed Tetrahydrofuran Formation via Dual Pathways in Avermectin Biosynthesis

Tianjian Sun,<sup>#</sup> Mingyu Liu,<sup>#</sup> Shuai Li, Jiawei Guo, Lei Liu, Lixin Zhang, Li Ma,<sup>\*</sup> and Shengying Li<sup>\*</sup>



Cite This: *ACS Catal.* 2025, 15, 3295–3305



Read Online

ACCESS |



Metrics & More



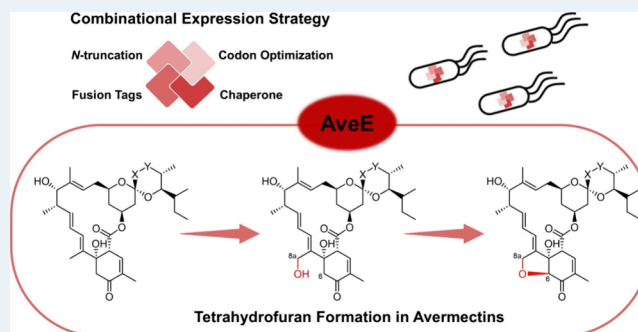
Article Recommendations



Supporting Information

**ABSTRACT:** Avermectins (AVMs) are a class of 16-membered ring macrolides produced by *Streptomyces avermitilis*. Renowned for their potent insecticidal and acaricidal properties, AVMs are widely used as environmentally friendly biopesticides. Although the biosynthetic gene *aveE* encoding a cytochrome P450 monooxygenase was identified 30 years ago, its exact catalytic function and mechanism have remained elusive due to a lack of biochemical characterization. Here, we overcome the long-standing challenge in soluble and functional protein expression of AveE in *Escherichia coli* and reconstitute the *in vitro* activity of this P450 enzyme using surrogate redox partner proteins. Time-course studies reveal monohydroxylation at the C8a position of the substrates as the initial step, subsequently leading to tetrahydrofuran (THF) ring formation. Isotopic labeling experiments provide significant insight into the catalytic mechanism of AveE, revealing the cooperation of the C8a,C6-diol pathway and the C6-nucleophilic attack pathway. This study not only presents an effective strategy for heterologous expression of difficult P450 enzymes in *E. coli* but also elucidates the exact process of THF ring formation during AVM biosynthesis.

**KEYWORDS:** avermectins, biosynthesis, cytochrome P450 enzymes, AveE, tetrahydrofuran



## INTRODUCTION

Substituted oxygen-containing heterocycles (*O*-heterocycles) are important structural components frequently present in polyketides and many other natural products (Figure 1).<sup>1</sup> These *O*-heterocycles, typically spanning from three- to six-membered rings, can impart rigidity to the carbon backbone and enhance the biological and pharmacological properties of the final products. Among diverse *O*-heterocyclic moieties, the five-membered rings—particularly fused or bridged tetrahydrofuran (THF)—hold an exceptional position in polyketide natural products.<sup>2,3</sup> Over the past few decades, a growing number of THF-containing polyketides have been discovered from both terrestrial and marine sources. With a wide spectrum of bioactivities, including antitumor, antimicrobial, antiprotozoal, antimalarial, and antihelminthic effects, their potential to be developed into new therapeutic agents has rapidly expanded.<sup>4</sup>

The intriguing THF structural feature is exemplified by the endectocides avermectins (AVMs) and their natural structural analogues including meilingmycins (MEIs), milbemycins (MILs), and nemadectin (NEM) (Figure 2B and Figure S1).<sup>5</sup> AVMs produced by *Streptomyces avermitilis* constitute a series of antiparasitic 16-membered macrocyclic polyketides.<sup>6</sup> The AVM family comprises eight members distinguished by the permutation of three structural variations: methoxylation (A series) or hydroxylation (B series) at C5, a double bond

between C22 and C23 (1 series) or its hydrated product at C23 (2 series), and substitution with methylpropyl (a series) or isopropyl (b series) at C25. Renowned for their potent anthelmintic activity and minimal toxicity in humans and animals, AVMs are widely used in the control of parasites in domestic animals and treatment of agricultural parasitic diseases.<sup>7,8</sup> Notably, AVMs serve as the precursor compounds of the Nobel Prize recognized anthelmintic drug ivermectin (22,23-dihydro-avermectin B<sub>1</sub>), which has revolutionized the treatment of human endo- and ectoparasitic diseases, including onchocerciasis (river blindness), lymphatic filariasis (elephantiasis), strongyloidiasis, and trichuriasis.<sup>9,10</sup>

The biosynthetic pathway of AVMs has been extensively studied since the type-I polyketide synthase (PKS) building blocks were identified through <sup>13</sup>C and <sup>18</sup>O labeling studies in 1983 (Figure 2).<sup>11</sup> The assembly of the biosynthetic gene cluster (BGC) of AVMs in 1999 and publication of the complete genome sequence of the industrial AVM-producing *S. avermitilis* ATCC 31267 in 2001 have significantly advanced

Received: November 8, 2024

Revised: January 29, 2025

Accepted: January 30, 2025

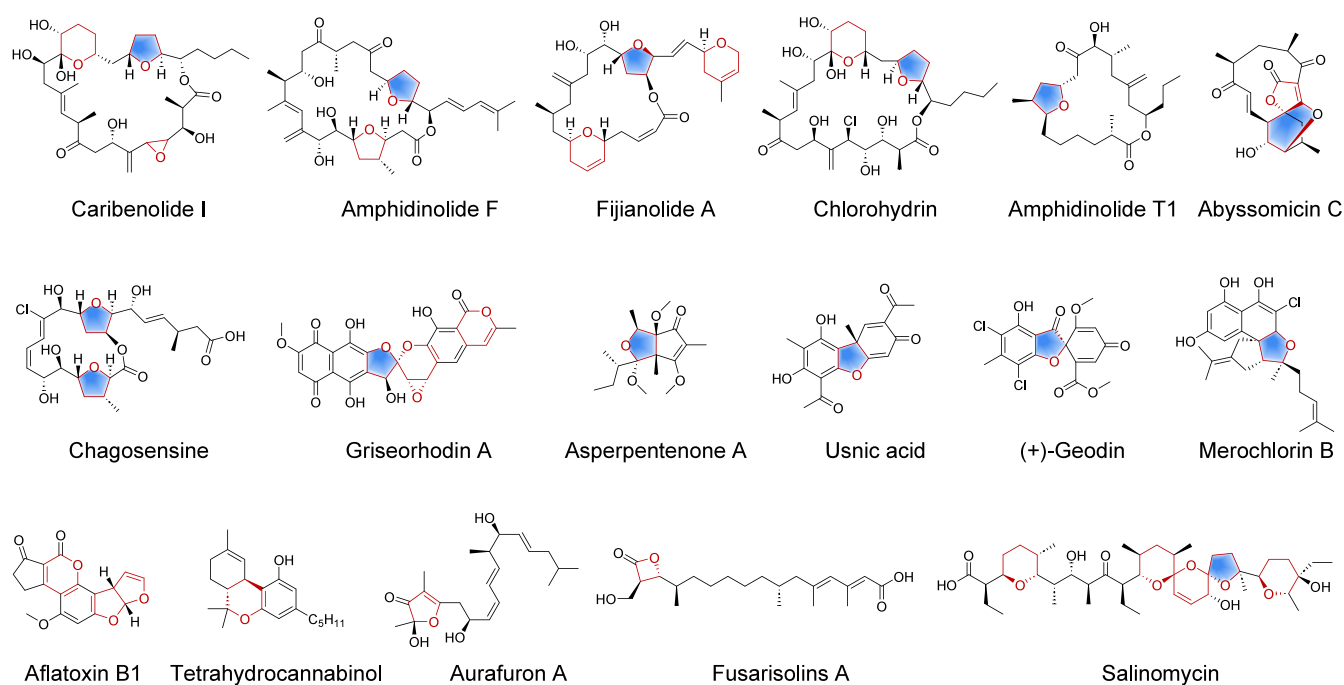


**Figure 1.** Representatives of *O*-heterocycle (in red) containing polyketides. The tetrahydrofuran (THF) moieties are shaded in blue.

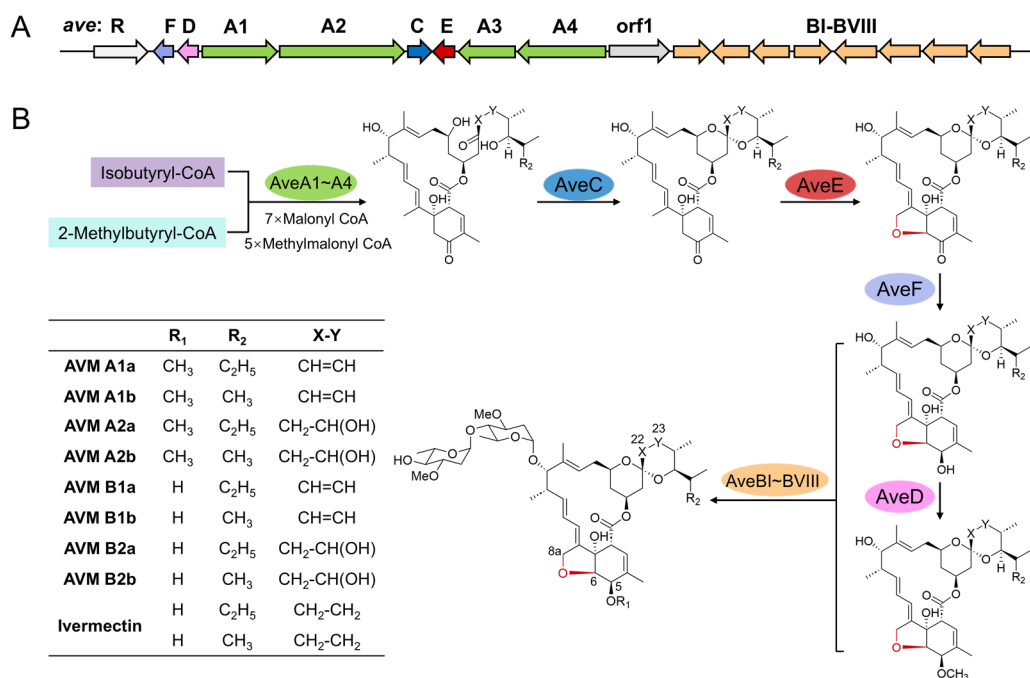


**Figure 2.** Structures and biosynthesis of avermectins (AVMs, comprising eight naturally occurring members, as shown in the embedded table). (A) Biosynthetic gene cluster of AVMs. (B) Biosynthetic pathway of AVMs with the P450 AveE-mediated tetrahydrofuran formation highlighted in red.

our understanding and enabled the targeted engineering of AVM biosynthesis.<sup>12,13</sup> The 16-membered ring macrolactone skeleton of AVMs is assembled from isobutyryl-CoA/2-methylbutyryl-CoA starter units and malonyl-CoA/methylmalonyl-CoA extender units by a modular PKS system (AveA1–A4).<sup>12</sup> For post-PKS tailoring modifications, AveC mediates the spirocyclization and optional dehydration at the C22–C23 position.<sup>14</sup> AveF and AveD catalyze the ketoreduction and *S*-adenosyl methionine (SAM)-dependent methylation at C5, respectively.<sup>15–17</sup> AveBI–BVIII (also referred to as AvrC–AvrI) are essential for the synthesis and attachment of TDP-β-

*L*-oleandrose.<sup>18,19</sup> The THF ring, a key pharmacophore of AVMs, is considered to be installed by the P450 enzyme AveE (*i.e.*, CYP171A1). Previous *in vivo* studies, including *aveE* knockout and complementation analyses, and precursor bioconversion experiments have indicated that the ring closure at C6–C8a necessitates the presence of a keto group at the C5 position.<sup>20</sup> In addition, both AveF and AveBI exhibit high substrate promiscuity, functioning either preceding or subsequent to AveE in the biosynthetic cascade.<sup>20–22</sup> Notwithstanding these insightful findings, the exact catalytic

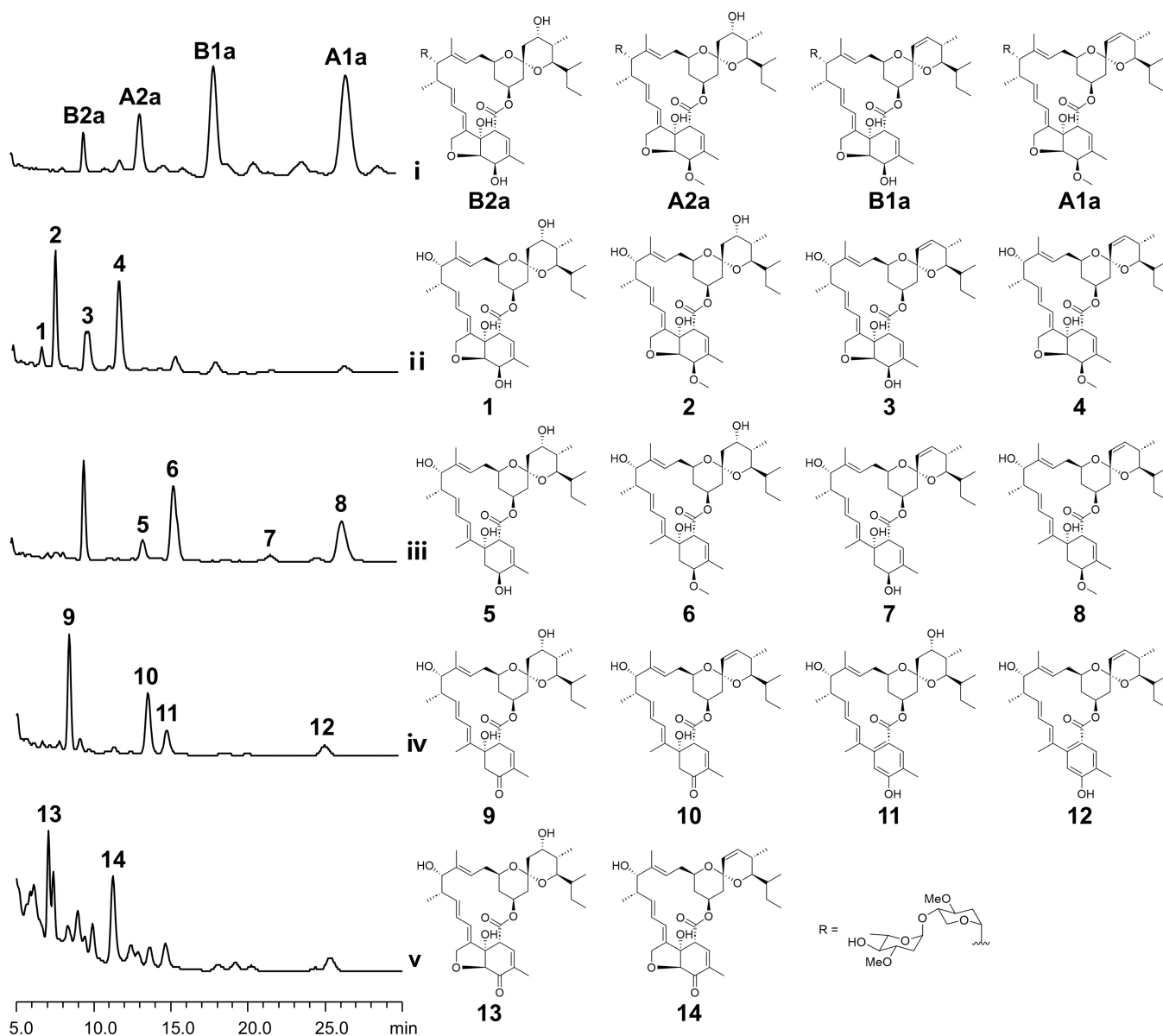


**Figure 3.** HPLC analysis (240 nm) of the metabolites of *S. avermitilis* knockout mutant strains. (i) 9-39-WT (SA001); (ii) 9-39- $\Delta$ *aveBI* (SA002); (iii) 9-39- $\Delta$ *aveBI*- $\Delta$ *aveE* (SA003); (iv) 9-39- $\Delta$ *aveBI*- $\Delta$ *aveE*- $\Delta$ *aveF* (SA004); (v) 9-39- $\Delta$ *aveBI*- $\Delta$ *aveF* (SA005). Structures of the products isolated from the fermentation cultures of SA001–SA005 are shown in the right panel.

function and mechanism of AveE remain hitherto to be firmly established.

Despite decades of research efforts, the unavailability of the purified functional AveE protein has been hindering the deeper understanding of this intriguing P450 enzyme. Unusually, AveE exhibits low similarity with other known P450 monooxygenases involved in furan tailoring (Figure S2), such as AurH (CYP151A family) from *Streptomyces thioluteus* (21% identity), crotonolide G synthase SdCS (CYP76AH39) from *Salvia divinorum* (22% identity), and PtmO5 from *Streptomyces platensis* SB12029 (24% identity).<sup>23–25</sup> Furthermore, AveE homologues in the biosynthetic pathways of MILs, MEIs, and NEM, namely, MilE (60% identity), MeiE (61% identity), and NemE (75% identity), which are likely to have similar functions to AveE, yet remain largely unexplored perhaps owing to similar problems of soluble protein expression. Therefore, elucidation of AveE's function and mechanism will not only contribute to broadening our

understanding of P450-catalyzed *O*-heterocyclization but also facilitate the study of homologous proteins. Herein, an effective strategy for the soluble and functional expression of AveE in *Escherichia coli* was established. With this breakthrough, we for the first time provided direct *in vitro* experimental evidence of AveE's activity and elucidated the catalytic details of THF ring formation during the biosynthesis of AVMs.

## RESULTS

**Analysis of the Metabolic Profiles of *aveE* Knockout Mutants.** We cultured the AVM high-producing strain *S. avermitilis* 9-39 (termed SA001 in this study) in fermentation medium for 7 days and detected four main AVM products, namely, AVMs B2a, A2a, B1a, and A1a.<sup>26</sup> To prepare the substrates of AveE, the genes encoding the tailoring enzymes AveE, AveF, and AveBI were targeted for gene knockout in order to block the AveE-mediated step and downstream modifications, thereby enabling substrate accumulation (Figure

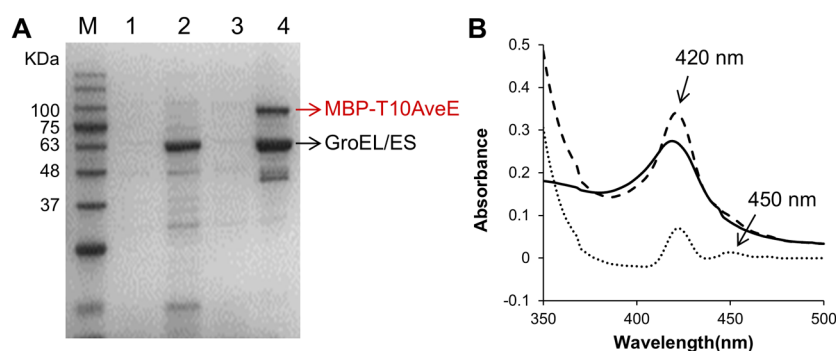


**Figure 4.** SDS-PAGE gel analysis and characteristic absorption spectral analysis of AveE. (A) M: marker; lane 1: GroEL/ES chaperonin complex before induction; lane 2: GroEL/ES after induction; lane 3: MBP-T10AveE before induction; lane 4: purified MBP-T10AveE protein (90.8 kDa). (B) Characteristic absorption spectra of MBP-T10AveE: the oxidized ferric form (solid line), the  $\text{Na}_2\text{S}_2\text{O}_4$ -reduced ferrous-CO complex (dashed line), and the reduced difference spectrum (dotted line).

3). Given that the genome of strain SA001 contains a duplicate copy of the AVM BGC according to the genome sequencing result (Figure S3), we employed the CRISPR-cBEST (CRISPR-Base Editing SysTem with a cytidine-based base editor) for AVM biosynthetic gene knockout (Figures S4 and S5), which has been proven efficient in simultaneously inactivating duplicated genes in *Streptomyces* BGCs.<sup>27</sup> Initially, we knocked out the two copies of the *aveBI* gene at once (same below), resulting in a single mutant strain 9-39- $\Delta$ *aveBI* (SA002), which yielded intermediates 1–4. According to high-resolution mass spectrometry (HRMS) analysis, these compounds were characterized as the aglycones of AVMs B2a, A2a, B1a, and A1a, respectively (Figure S6).

Next, we deleted *aveE* from SA002 to construct the 9-39- $\Delta$ *aveBI*- $\Delta$ *aveE* double knockout strain (SA003). This strain completely lost the ability to synthesize the THF-containing AVMs, instead producing compounds 5–8 without any oxidative modification at the position of C8a. None of the eight AVM-related products of SA002 and SA003 bore a carbonyl group at C5 site, corroborating the catalytic promiscuity of the ketone reductase AveF on both THF-containing and THF-free substrates as previously reported.<sup>14</sup> Thus, we further inactivated *aveF* from strain SA003 to construct the 9-39- $\Delta$ *aveE* $\Delta$ *aveF* $\Delta$ *aveBI* triple knockout strain (SA004). The resulting strain yielded 9 and 10 with unreduced carbonyl groups at C5 when compared to 5 and 6, respectively. The NMR and HRMS spectra were virtually identical to the reported ones.<sup>14,20</sup> Concurrently, two new products 11 and 12 with lower polarities were detected. According to NMR and HR-MS data, 11 and 12 appeared to be the spontaneous dehydration derivatives of 9 and 10 (Figures S6, S7, and S28–39), respectively. Additionally, the 9-39- $\Delta$ *aveF* $\Delta$ *aveBI* double-knockout strain (SA005) was constructed, yielding the THF-containing product 13 and 14. Strains SA004 and SA005 were cultured in large-scale fermentation (approximately 20 L of culture broth) to isolate and purify compounds 9, 10, 13, and 14, which were utilized in the following *in vitro* biochemical experiments.

#### **In Vitro Expression and Spectral Properties of AveE.**

Heterologous soluble expression of AveE has long posed a significant challenge since its encoding gene was identified 30 years ago.<sup>20</sup> This difficulty might be attributed to several factors, including the mismatch between the codon usage of the heterologous host and original *aveE* gene, incorrect protein folding, and improper disulfide bond formation in heterologous hosts.<sup>28</sup> To address these issues and achieve soluble

expression of the functional AveE protein in *E. coli*, we adopted various strategies. First, we constructed a pCWori-*aveE* plasmid (containing double *tac* promoters) with a synthetic codon-optimized *aveE* gene, which was subsequently transformed into the *E. coli* JM109 (DE3) strain. However, this approach yielded only a minimal P450 expression. The protein structure prediction using AlphaFold 3 indicated that the *N*-terminal 10 amino acids of AveE are in a random coil conformation (Figure S8).<sup>29</sup> Considering the potential negative impact of the *N*-terminal flexible region on protein folding, we truncated these 10 amino acids, resulting in enhanced protein expression of the *N*-truncated form of AveE (i.e., T10AveE, Figure S9A). Despite this improvement, purification of soluble T10AveE via Ni-NTA affinity chromatography was still unsuccessful.

To further enhance soluble protein production, the strategy of adding fusion tags was attempted, which has been known to be useful for solubility improvement.<sup>30</sup> Specifically, we fused AveE with various tags to its *N*-terminus, including maltose binding protein (MBP), small ubiquitin-like modifier (SUMO), glutathione *S*-transferase (GST), thioredoxin A (TrxA), and disulfide oxidoreductase (DsbA). Among these, MBP turned out to be the most effective choice, enhancing both the yield and the quality of soluble AveE production (MBP-T10AveE) (Figure S9B). Chaperones, such as Trigger Factor, GroEL, and Heat Shock Proteins 60, play crucial roles in protein folding, assembly, and translocation under both physiological and stress conditions.<sup>31</sup> Thus, we further tested the ability of these chaperones to assist AveE expression and folding and found GroEL as the most effective one. By harnessing this combined expression approach and optimizing culture conditions, we eventually achieved considerable soluble expression of AveE. The MBP-T10AveE proteins were purified to homogeneity using Ni-NTA agarose and starch resin stepwise (Figure 4A). To evaluate the effectiveness of this protein expression strategy, we also applied it to the homologous P450 enzyme MeiE from *Streptomyces nanchangensis*, which was also known for its difficulty in achieving soluble heterologous expression.<sup>32</sup> Using the same method and conditions as those developed for AveE, we successfully expressed MeiE in *E. coli* JM109 (DE3) (Figure S10A).

P450 enzymes are typically characterized by the Soret peak around 450 nm in their CO-bound reduced difference spectra.<sup>33</sup> However, such spectra of AveE and MeiE only showed a minor peak near 450 nm, with the maximum absorption of the  $\text{Fe}^{2+}$ -CO complex at around 420 nm (Figure

4B and Figure S10B). This unusual spectral property might result from either protonation of the proximal cysteine sulfur ligand to its neutral thiol state or from dissociation of the sulfur ligand from the heme iron, followed by binding to an alternative proximal ligand (such as histidine), or from other reduction-linked structural changes that prevent the formation of thiolate-ligated  $\text{Fe}^{2+}$ -CO species.<sup>34–36</sup>

Next, we expressed and purified several soluble endogenous redox partners of *S. avermitilis* 9–39, including three ferredoxins (Fdxs including FdxA, FdxC, and FdxF) and two ferredoxin reductases (FdxRs including FdxRE and FdxRD) (Figure S11). Unexpectedly, none of the combinations of purified native Fdxs and FdxRs supported the activity of AveE *in vitro* (Figure S12) for unknown reasons. Prokaryotic redox partner systems are diverse and complex, typically consisting of multiple Fdxs and FdxRs that fall into different categories.<sup>37,38</sup> The inability of these endogenous redox partners to support the activity of recombinant AveE likely arises from the limited scope of the native redox partners tested. While *S. avermitilis* 9–39 encodes nine Fdxs and six FdxRs, only three Fdxs and two FdxRs were successfully expressed in *E. coli*, preventing the full identification of suitable endogenous redox partners for AveE. Thus, instead of the native redox partner proteins, a universally efficient surrogate Fdx/FdxR system (*i.e.*, SelFdxR0978 and SelFdx1499) from the cyanobacterium *Synechococcus elongatus* PCC 7942 was employed to reconstitute the *in vitro* activity of AveE.<sup>39,40</sup> Additionally, glucose dehydrogenase (GDH) was used for establishing a NADPH regeneration system with glucose as the electron source.<sup>41</sup>

**Characterization of the THF-Forming Activity of AveE.** We incubated potential substrate **9** with purified MBP-T10AveE, SelFdxR0978, SelFdx1499, GDH, glucose, and NADPH at 30 °C for 3 h. The P450 reaction yielded three products, namely, **13**, **15**, and **16**. The product **13** (Figure 5B) exhibited identical HPLC retention time, and UV-vis, NMR, and HRMS spectra to the standard **13** isolated from SA005 fermentation cultures. To determine the structures of **15** and **16**, we scaled up the enzymatic reaction system (50 mL) to isolate these two products for NMR and HRMS analyses. Product **15** ( $[\text{M} + \text{Na}]^+$ ,  $m/z$ : obs. 625.3342, calc. 625.3353 for  $\text{C}_{34}\text{H}_{50}\text{O}_9$ ) showed a 16 Da increase in molecular weight compared to **9**. The NMR spectra of **15** closely resembled those of **9**, except for a change at C8a from methyl to methylene with a  $^{13}\text{C}$  chemical shift of 58.4 (Table S5). These data indicated that **15** should be the monohydroxylation product of **9** at the C8a position. Of note, compound **15** was unstable, readily converting to the stable compound **16**. Compound **16** ( $[\text{M} + \text{Na}]^+$ ,  $m/z$ : obs. 607.3247, calc. 607.3247 for  $\text{C}_{34}\text{H}_{48}\text{O}_8$ ) exhibited a decrease in molecular weight by 18 Da compared to **15**, indicating that **16** should be the dehydration derivative of **15**. This transformation was also observed in the enzyme-free negative controls, suggesting that it likely occurred spontaneously. For substrate **10**, a similar pattern of products were detected, including the THF-bearing product **14**, the unstable monohydroxylation product **17**, and the spontaneous dehydration product **18**. The characteristic  $^{13}\text{C}$  chemical shifts of aromatic carbons (ranging from 116.1 to 159.0 ppm) in compound **18** strongly supported the idea that dehydration should occur between C2 and C7 (Table S6). This dehydration would facilitate the keto-enol tautomerism at C5, ultimately forming a stable benzene ring moiety. Of note, similar dehydrative aromatization of the C2–C7 ring was previously reported in spiral ring-opened aglycones of AVMs.<sup>14</sup>

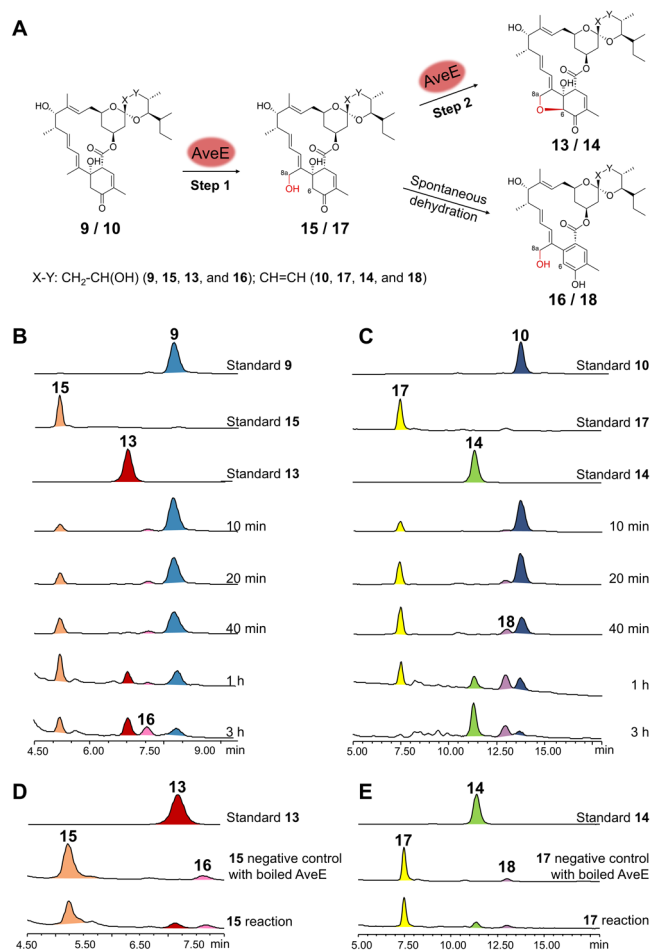


**Figure 5.** AveE-catalyzed reactions. (A) Schematic reactions catalyzed by AveE. (B) Time-course experiments of AveE with **9** as the substrate. (C) Time-course experiments of AveE with **10** as substrate. (D) 1 h reaction of AveE with **15** as the substrate. (E) 1 h reaction of AveE with **17** as substrate. The typical 100  $\mu\text{L}$  reaction mixture containing 5  $\mu\text{M}$  AveE, 10  $\mu\text{M}$  selFdx1499, 5  $\mu\text{M}$  selFdxR0978, 100  $\mu\text{M}$  substrate, 1 mM NADPH, 10 mM glucose, and 2 U GDH was performed at 28 °C. HPLC analyses were conducted at 240 nm.

To better understand the AveE-mediated enzymatic conversion process, time-course experiments were conducted and analyzed by HPLC (Figure 5). Over a time range of 10 to 40 min, we observed accumulation of monohydroxylation intermediates **15** and **17**, along with their spontaneous dehydration derivatives **16** and **18**, respectively. Subsequently, the quantities of compounds **15** and **17** decreased, while THF-containing products **13** and **14** and dehydration derivatives **16** and **18** accumulated (Figure 5B,C). Thus, the formation of **13** and **14** appears to be a two-step process that includes C8a hydroxylation and subsequent heterocyclization, thereby generating the THF ring. However, it remains to be determined whether compounds **15** and **17** are indeed the intermediates and whether the second step of the reaction is enzyme-driven or spontaneous. Thus, we next used the isolated monohydroxylation products **15** and **17** as substrates for AveE catalysis, where the production of **13** and **14** was clearly identified. By contrast, in the negative control with boiled AveE, only the dehydration shunt products **16** and **18** were generated (Figure 5D,E). These results clearly demonstrate that the biosynthesis of the THF ring in AVMs should be a P450-mediated two-step process.

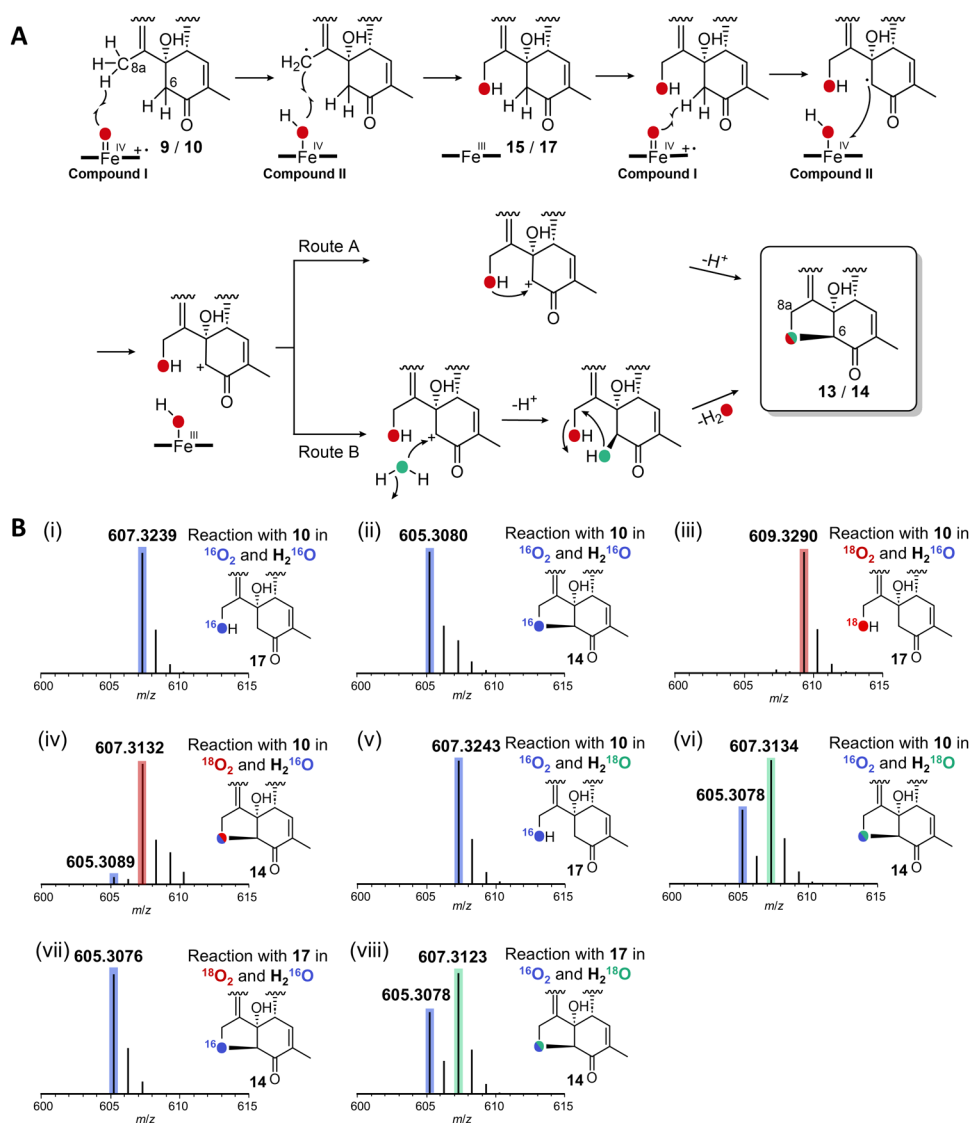


**Figure 6.** Elucidation of the mechanisms for THF ring formation catalyzed by AveE. (A) Schematic mechanisms of AveE. (B) Isotopic labeling analysis of AveE-mediated reactions using substrates **10** and **17**. For the AveE reactions with substrate **10**: mass spectra of product **17** (i) and product **14** (ii) in  $^{16}\text{O}_2$  and  $\text{H}_2^{16}\text{O}$ ; product **17** (iii) and product **14** (iv) in  $^{18}\text{O}_2$  and  $\text{H}_2^{16}\text{O}$ ; product **17** (v) and product **14** (vi) in  $^{16}\text{O}_2$  and  $\text{H}_2^{18}\text{O}$ . For the AveE reactions with substrate **17**: mass spectra of product **14** in  $^{18}\text{O}_2$  and  $\text{H}_2^{16}\text{O}$  (vii) and in  $^{16}\text{O}_2$  and  $\text{H}_2^{18}\text{O}$  (viii). Positive molecular ions are indicated. The oxygen atoms incorporated from  $^{16}\text{O}_2$  and  $\text{H}_2^{16}\text{O}$  are highlighted in blue, from  $^{18}\text{O}_2$  in red, and from  $\text{H}_2^{18}\text{O}$  in green.

In our *in vitro* assays, both substrates and monohydroxylated intermediates rapidly degraded into dehydration derivatives spontaneously, hindering our structural identification. A similar transformation was observed in the previous study of AveC.<sup>14</sup> Due to inherent instability of these substrates and intermediates, we reason that the AveE-catalyzed *O*-heterocycle formation plays a pivotal role in guiding AVM biosynthesis. By production of more stable THF-containing intermediates, this enzymatic outcome would avoid the generation of undesirable dehydration shunt products.

To further investigate enzyme–substrate interactions, we measured the binding affinities of substrates **9**, **10**, **15**, and **17** through UV-visible absorption titrations.<sup>42</sup> The dissociation constant ( $K_D$ ) values for substrates **9** and **10** with AveE were determined to be  $1.3 \pm 0.2$  and  $1.8 \pm 0.2 \mu\text{M}$ , respectively, indicating strong binding affinities that support the occurrence of the initial C8a hydroxylation step. In contrast, due to the instability of **15** and **17** or other unknown reasons, their

titration curves were unsuitable for reliable  $K_D$  calculation (Figure S13).

**Mechanism of THF Ring Formation.** Based on experimental observations, we proposed a putative catalytic mechanism for the THF ring formation mediated by P450 AveE. In the initial step, AveE abstracts a hydrogen atom from the C8a allylic position of **9** or **10**, generating a C8a carbon radical. This is followed by the rebound of the hydroxyl group on the  $[\text{Fe}^{\text{IV}}\text{OH}]$  intermediate to the substrate radical, yielding the C8a-hydroxylated product **15** or **17**. Subsequently, the second activation cycle occurs, and the AveE ferryl-oxo species (compound I) abstracts a hydrogen atom from the C6 methylene, producing a C6 carbon radical followed by another electron abstraction by compound II, giving rise to a carbocation. Next, two potential pathways are proposed. In route A, C8a–OH directly attacks the carbocation at C6, leading to cyclization and formation of the THF ring with concomitant deprotonation. Due to the inherent chemical

stability of the *cis* conformation of the five-membered ring attached to cyclohexene, the THF ring is formed with *S*-configuration at C6 exclusively. In route B, hydroxylation occurs at C6 via attack by a water molecule, leading to a hydroxylated C6 with an *S*-configuration. The C8a allylic position then undergoes nucleophilic attack by the hydroxyl group at C6, forming the THF ring with the release of a water molecule (Figure 6A).

To distinguish these two alternative mechanisms, we conducted isotopic labeling experiments with H<sub>2</sub><sup>18</sup>O and <sup>18</sup>O<sub>2</sub> in AveE assays, using compounds **10** and **17** as substrates. The molecular masses of the resulting oxidized products were analyzed by LC-HRMS, with products from the reaction with substrate **10** in <sup>16</sup>O<sub>2</sub> and H<sub>2</sub><sup>16</sup>O serving as references (Figure 6B, traces i and ii). When compound **10** was used as a substrate, the <sup>18</sup>O<sub>2</sub> assay showed a complete shift in the [M + Na]<sup>+</sup> ion of intermediate **17** from *m/z* 607 to 609 (Figure 6B, trace iii), indicating that the oxygen atom in C8a hydroxylation should originate from molecular oxygen. A mixture of [M + Na]<sup>+</sup> ions at *m/z* 605 and 607 was observed for compound **14** (Figure 6B, trace iv), suggesting the co-occurrence of routes A and B. In the H<sub>2</sub><sup>18</sup>O assay, no shift was observed in the [M + Na]<sup>+</sup> ion of compound **17**, but a partial shift from *m/z* 605 to 607 was detected in compound **14** (Figure 6B, traces v and vi). This two-Dalton shift indicated that a hydroxylation at C6 with the <sup>18</sup>O atom originated from H<sub>2</sub><sup>18</sup>O occurred through a C6 carbocation intermediate, followed by the C8a-<sup>16</sup>OH elimination via dehydration, as proposed in route B. Notably, approximately 60% of product **14** in this H<sub>2</sub><sup>18</sup>O assay displayed <sup>18</sup>O incorporation, leaving open the possibility that the C6 carbocation could also be directly trapped by the hydroxy group at C8a (route A).

With compound **17** as the substrate in the <sup>18</sup>O<sub>2</sub> assay, no shift in the [M + Na]<sup>+</sup> ion of compound **14** was detected (Figure 6B, trace vii), further supporting that the C6 hydroxylation likely involves a C6 carbocation intermediate instead of via oxygen rebound. In the H<sub>2</sub><sup>18</sup>O assay, a partial shift in the [M + Na]<sup>+</sup> ion of **14** from *m/z* 605 to 607 was observed (Figure 6B, trace viii), supporting our hypothesis. Of note, when compounds **10**, **14**, and **17** were incubated in H<sub>2</sub><sup>18</sup>O for 24 h, MS analysis showed no detectable incorporation of the <sup>18</sup>O atom, confirming that no oxygen exchange occurred between these compounds and water (Figure S14). Taken together, these <sup>18</sup>O<sub>2</sub> and H<sub>2</sub><sup>18</sup>O labeling experiments demonstrated that routes A and B contribute cooperatively through a common C6 carbocation intermediate.

## DISCUSSION

Furan-containing compounds, including AVMs, are not uncommon in nature, where furan formation imparts substantial chemical and biological properties. These five-membered *O*-containing heterocycles are biosynthesized by a variety of enzymes, such as P450 enzymes, copper proteins,  $\alpha$ -KG-dependent oxygenases, and flavoenzymes.<sup>43</sup> P450 enzymes, a superfamily of heme-thiolate proteins, have only a few members characterized so far for furan ring synthesis, and their catalytic mechanisms remain underexplored.<sup>44–46</sup> Notable examples include AurH in aureothin biosynthesis, SdCS in dihydrofuran neoclerodane biosynthesis, and PtmO5 in platensimycin biosynthesis.<sup>23–25</sup> Mechanistically, AurH initially oxidizes the C7 methylene of the aureothin precursor to generate an *R*-configured monohydroxylation intermediate and

then catalyzes the formation of a second C–O bond to form a THF ring. It remains unclear whether a transient dihydroxylated or allylic radical intermediate at C9a is involved in the heterocyclization process (Figure S15). In the other two cases, the biosynthetic pathways proceed preferentially through a dihydroxylated intermediate.<sup>5</sup> For SdCS, <sup>18</sup>O<sub>2</sub> feeding experiments indicated that furan formation in crotonolide **G** is achieved via a dihydroxylated intermediate. SdCS incorporates an aerobic oxygen into C16 of kolavenol, followed by protonation of C15–OH and loss of water to generate an allylic cation at C15, which is then attacked by the OH at C16.<sup>24</sup> For PtmO5, the absolute configuration of the furan ring in platensimycin suggests an 11*S*,16*R*-diol intermediate, with the 11*S*,16*S*-furan ring formed by intramolecular dehydration.<sup>25</sup> Our sequence analysis revealed that AveE shows low degree of sequence identity/similarity with AurH, SdCS, and PtmO5 (Figure S2). AveE is phylogenetically distinct yet functionally analogous to these P450s, indicative of convergent evolution. However, based on our labeling experiments, the mechanism for THF formation in AVMs diverges notably from previously described pathways. This mechanism involves a crucial C6 carbocation intermediate, through which THF ring formation proceeds via both the C8a,C6-diol pathway and the C6-nucleophilic attack pathway. Further structural and computational studies of AveE are required to elucidate the detailed mechanism, which are currently ongoing in this laboratory.

Despite being identified 30 years ago, the exact function and mechanism of the representative enzyme AveE remain largely unexplored. This lack of understanding was primarily due to difficulties in preparing soluble proteins and analyzing unstable intermediates. Achieving a heterologous soluble expression of *Streptomyces* P450s sometimes is challenging for unclear reasons, and there is not any universal guideline to follow. It usually relies on understanding the features of specific protein types and extensive trial-and-error experimentations. In addition to AveE, there are still a number of prokaryotic P450s that are difficult to express and purify from a heterologous expression host (e.g., *E. coli*) or exhibit activity insufficient for practical biocatalysis. For example, VenC, which catalyzes carbonylation in venezuelaene B biosynthesis, has yet to be expressed in a functional and soluble form.<sup>47,48</sup> AveE homologues, including MilE and NemE, have also faced similar expression issues, further hampering the *in vitro* biochemical study and structural characterization. To overcome the expression challenge associated with AveE, herein, we developed a combinational expression approach that included codon optimization, *N*-terminal truncation, MBP-tag fusion, and the use of the pGro12 chaperone. This approach successfully enabled the production of soluble AveE (along with its homologue MeiE) in *E. coli* and facilitated the investigation of its catalytic characteristics in greater detail. This work not only provides valuable insight into AveE's function and mechanism but also serves as a useful reference for expressing other problematic P450 proteins, marking an important step in overcoming the barrier of heterologous protein expression.

## CONCLUSIONS

In this study, we successfully achieved the soluble expression and purification of P450 AveE in *E. coli* and reconstituted its activity *in vitro* for the first time. Through biochemical assays, we demonstrated that this single P450 monooxygenase is

capable of installing at least two C–O bonds sequentially. We provide the first direct evidence of AveE-catalyzed THF formation within AVM biosynthesis and reasonably propose possible catalytic mechanisms based on isotopic labeling experiments. This work offers an experimental foundation for comprehending the THF ring formation process in AVMs and their analogs and serves as an example for investigating the unusual roles of P450 enzymes in O-heterocycle formation. Moreover, the detailed characterization of AveE paves the way for applying AveE chemistry to rational engineering of relevant pathways to selectively produce a THF moiety for potential pharmaceutical use.

## METHODS

**Materials.** Unless otherwise specified, biochemicals were purchased from Sinopharm Chemical Reagent Co., Ltd. (China), or Shanghai Aladdin Biochemical Technology Co., Ltd. (China). Media and antibiotic were bought from Beijing Solarbio Science & Technology Co., Ltd. (China), or Taiwan Biotech Co., Ltd. (China). Chemical reagents were obtained from standard commercial sources. DNA polymerases were purchased from Takara Biotechnology Co., Ltd., and Nanjing Vazyme Biotech Co., Ltd. Kits for plasmid extraction and DNA purification were supplied by Omega Bio-tek (Norcross, Georgia, USA). DNA sequencing was performed by Sangon Biotech (Shanghai, China). His-tagged protein purification utilized Qiagen Ni-NTA resin (Valencia, California, USA).

**Strains and Culture Conditions.** The bacterial strains and plasmids used in this study are given in Table S1. *E. coli* strains were cultured at 37 °C on LB (10 g of tryptone, 5 g of yeast extract, and 10 g of NaCl per liter) or in LB liquid media. *S. avermitilis* 9-39 wild-type and knockout strains were grown at 30 °C on mannitol soya flour (MS) agar (20 g of soy flour, 20 g of mannitol, 20 g of agar per liter) for sporulation and conjugation. *E. coli* ET12567/pUZ8002 was employed for intergeneric conjugation with *S. avermitilis* in MS medium supplemented with 50 mM CaCl<sub>2</sub> and MgCl<sub>2</sub>. The seed medium composed of 30 g of corn starch, 8 g of soy bean cake powder, 10 g of peanut meal, 4 g of yeast extract, and 0.03 g of CoCl<sub>2</sub> per liter at pH 7.0 was employed for the cultivation of *S. avermitilis* liquid seed and for the preparation of genomic DNA (gDNA). The fermentation medium (150 g of corn starch, 25 g of soy bean cake powder, 10 g of yeast extract, 0.5 g of CaCO<sub>3</sub>, 0.25 g of (NH<sub>4</sub>)<sub>2</sub>SO<sub>4</sub>, 0.02 g of Na<sub>2</sub>MoO<sub>4</sub>, 2.3 mg of MnSO<sub>4</sub>, and 0.2 g of CoCl<sub>2</sub> per liter, pH 7.0) was utilized for the production of AVMs.

**DNA Manipulations and Sequence Analyses.** The primers used in this work are given in Table S2. Standard protocols were used for DNA purification, PCR, and molecular cloning. DNA synthesis and sequencing were carried out at Sangon Biotech (Shanghai, China). PCR was conducted using 2× Phanta Mix Super-Fidelity (Nanjing Vazyme Biotech) and PrimeSTAR Max DNA polymerase (Takara Biotech). DNA digestion was carried out using FastDigest restriction enzymes (Thermo Fisher Scientific). To employ pCRISPR-cBEST for base editing applications, a 20 nt spacer was integrated into the sgRNA scaffold. The CRISPy web tool (<https://crispy.secondarymetabolites.org>) was utilized to design the spacer (Table S3). The constructed plasmid was transformed into *E. coli* ET12567/pUZ8002 cells and subsequently into *S. avermitilis*. Eight clones were directly sequenced using primers “pCRISPR-cBEST-YZ-FP” and “pCRISPR-cBEST-YZ-RP” to screen for the correct constructs. The DNA fragment encoding

*aveE* was amplified by PCR using synthesized primers from *S. avermitilis* gDNA. The truncated *aveE* gene (codon optimized) was connected to an MBP tag on the N-terminus and then subcloned into the pCWori vector. This recombinant plasmid was transformed into the *E. coli* JM109 (DE3) strain for protein expression.

**Protein Expression and Purification.** For the expression of P450 AveE, *aveE* was coexpressed with the *E. coli* molecular chaperone GroEL/ES in *E. coli* JM109 (DE3). All of the redox partners were expressed in *E. coli* BL21 (DE3) and purified with an N-terminal His-tag. A colony of the recombinant cell was inoculated into LB broth and grown at 37 °C, 220 rpm overnight. This culture was then transferred into 0.5 L of TB medium at a ratio of 1:100 (v/v) in a 2 L conical flask and incubated at 37 °C and 200 rpm for 4–6 h. Both the seed culture medium and fermentation culture medium required the addition of the antibiotic kanamycin (50 mg/L) or ampicillin (100 mg/L). Additionally, the fermentation culture medium was supplemented with a rare salt solution (25 μM FeCl<sub>3</sub>, 4 μM ZnCl<sub>2</sub>, 2 μM CoCl<sub>2</sub>, 2 μM Na<sub>2</sub>MoO<sub>4</sub>, 2 μM CaCl<sub>2</sub>, 3 μM CuSO<sub>4</sub> and 2 μM H<sub>3</sub>BO<sub>3</sub>).<sup>49</sup> Upon reaching an OD<sub>600</sub> of 0.6–0.7, the cells were induced by the addition of 0.4 mM isopropyl-β-D-1-thiogalactopyranoside (IPTG) and 0.5 mM δ-aminolevulinic acid (5-ALA). The cells were cultured at 18 °C for another 20 h and centrifuged at 6000g for 10 min to pellet cells. The following protein purification was carried out using Ni-NTA affinity chromatography as previously described.<sup>50</sup> The final purified proteins were flash frozen in liquid nitrogen and stored at –80 °C for subsequent use. The purified P450 AveE concentration was determined to be approximately 0.4 nmol/L based on its CO-bound difference spectrum ( $\epsilon_{450-490\text{ nm}} = 91,000\text{ M}^{-1}\text{ cm}^{-1}$ ).<sup>33</sup> The extinction coefficients of the flavin-bound SelFdxR0978 and the iron–sulfur containing SelFdx1499 were determined to be  $\epsilon_{454} = 19,120\text{ M}^{-1}\text{ cm}^{-1}$  and  $\epsilon_{460} = 11,270\text{ M}^{-1}\text{ cm}^{-1}$ , respectively.

**Chemical Analysis and Compound Preparation.** The HPLC analyses were conducted on a Thermo Scientific Dionex UltiMate 3000 system equipped with a YMC-Triart-C18 column (4.6 × 250 mm, 5 μm). Eluting was carried out by employing a mobile phase composed of methanol and deionized water with 0.1% formic acid at a flow rate of 1.0 mL/min. The gradient elution program of methanol in water was as follows: 0–30 min, 83%; 30–31 min, 83–100%; 31–35 min, 100%; 36–37 min, 100–83%; and 37–40 min, 83%. The column temperature was maintained at 25 °C, and the UV absorbance was detected at 240 nm. LC-ESI-HRMS analyses were carried out in positive ion mode on a Bruker impact HD High-Resolution Q-TOF mass spectrometer. Nuclear magnetic resonance (NMR) spectra were acquired by using a Bruker 600 MHz spectrometer (Bruker BioSpin GmbH Co., Rheinstetten, Germany), and the NMR data were processed by using MestReNova software.

The substrates of AveE, **9**, and **10** were prepared using mutant strain SA004. The double-knockout strain SA005 was constructed to prepare the THF-containing products of AveE (**13** and **14**). Strains SA004 and SA005 were fermented by following the procedure as described above. The culture broths of SA004 and SA005 were extracted twice with equal volumes of ethyl acetate. The extracts were then evaporated under vacuum and redissolved in methanol for product purification by semipreparative HPLC. The yields of compounds **9**, **10**, **13**, and **14** were 7.5, 10.0, 1.1, and 1.0 mg/L, respectively.

**P450 Substrate Binding Assay.** Purified P450 enzymes were diluted to a concentration range of 0.3 to 1.2  $\mu\text{M}$  using storage buffer (50 mM  $\text{NaH}_2\text{PO}_4$ , 200 mM NaCl, 10% glycerol, pH 7.3). Substrates were diluted to a series of concentrations between 0.5 and 10 mM with DMSO as stock solutions. The substrates dissolved at varying concentration gradients were titrated in equal volumes of 1  $\mu\text{L}$  at 25  $^\circ\text{C}$ . Difference spectra were recorded on a Molecular Devices Spectra Max<sup>M2</sup> spectrophotometer within the wavelength range of 350 to 500 nm. The difference absorbance  $\Delta A$  ( $A_{\text{peak}}(390\text{nm}) - A_{\text{trough}}(420\text{nm})$ ) values calculated from at least duplicated data were plotted against the substrate concentrations. Subsequently, the data points were fitted with the hyperbolic function of  $\Delta A = A_{\text{max}} [S]/(K_D + [S])$  using OriginPro 9.0, where  $A_{\text{max}}$  represents the maximum absorption shift at saturation,  $[S]$  denotes the total concentration of the substrate, and  $K_D$  is the apparent dissociation constant of the enzyme-substrate complex.

**P450 Enzymatic Assays.** The standard assay was composed of 5  $\mu\text{M}$  P450, 10  $\mu\text{M}$  *selFdx1499*, 5  $\mu\text{M}$  *selFdxR0978*, 100  $\mu\text{M}$  substrate, 1 mM NADPH, and the NAD(P)H regeneration system (10 mM glucose and 2 U GDH). The reaction was conducted in a 100  $\mu\text{L}$  volume of storage buffer. A preparative-scale reaction was performed in a 50 mL conical flask with a 10 mL reaction volume. The reactions were incubated at 30  $^\circ\text{C}$  for a certain period of time. The yields for the AveE reactions at specific time points were determined. For substrate **9**, after 3 h of reaction, the substrate conversion ratio was approximately 91%, with 30% yield for compound **15**, 48% yield for compound **13**, and 13% yield for compound **16**. For substrate **10**, after 1 h of reaction, the substrate conversion ratio was approximately 79%, with 33% yield for compound **17**, 19% yield for compound **14**, and 27% yield for compound **18**.

To quench the reactions, an equal volume of ethyl acetate was added. The extract was then evaporated and redissolved in methanol for HPLC and HRMS analyses. The samples were injected into Thermo Vanquish Duo UHPLC system coupled to a TSQ Triple Quadrupole Mass Spectrometer using a Thermo Accucore Polar Premium C18 column with the following program: isocratic flow of solvent A:solvent B = 80:20 for 40 min (A: HPLC-grade water with 0.1% formic acid; B: acetonitrile with 0.1% formic acid).

**$^{18}\text{O}_2$  and  $\text{H}_2^{18}\text{O}$  Labeling Experiments.** For the  $^{18}\text{O}_2$  labeling experiments, the reaction mixture was prepared in a degassed storage buffer containing 5  $\mu\text{M}$  AveE, 10  $\mu\text{M}$  *selFdx1499*, 5  $\mu\text{M}$  *selFdxR0978*, and 100  $\mu\text{M}$  substrate. Degassing was achieved by purging the buffer with nitrogen gas.  $^{18}\text{O}_2$  (98%, Icon Isotope) was introduced gently into the reaction vessel via a syringe needle connected to a compressed gas bag. To initiate the reaction, 1 mM NADPH dissolved in degassed storage buffer was added by using a microsyringe. The reaction vessel was immediately sealed and incubated at 30  $^\circ\text{C}$  for 2 h. For  $\text{H}_2^{18}\text{O}$  labeling experiments, the same reaction mixture was lyophilized to remove residual water. The freeze-dried components were rehydrated with  $\text{H}_2^{18}\text{O}$  (98%, Icon Isotope), and 1 mM NADPH dissolved in  $\text{H}_2^{18}\text{O}$  was added to initiate the reaction. The reaction vessel was sealed and incubated at 30  $^\circ\text{C}$  for 2 h. Postreaction processing and HPLC-MS analysis were conducted as described above.

## ■ ASSOCIATED CONTENT

### SI Supporting Information

The Supporting Information is available free of charge at <https://pubs.acs.org/doi/10.1021/acscatal.4c06900>.

Strains, plasmids, and primers; sequence alignment; predicted protein structure of AveE; SDS-PAGE gel analyses; spectral substrate binding data; HR-ESI-MS data; and NMR spectra (PDF)

## ■ AUTHOR INFORMATION

### Corresponding Authors

**Li Ma** – State Key Laboratory of Microbial Technology, Shandong University, Qingdao, Shandong 266237, China; [orcid.org/0000-0003-1601-7125](https://orcid.org/0000-0003-1601-7125); Email: maliqd@sdu.edu.cn

**Shengying Li** – State Key Laboratory of Microbial Technology, Shandong University, Qingdao, Shandong 266237, China; Laboratory for Marine Biology and Biotechnology, Qingdao Marine Science and Technology Center, Qingdao, Shandong 266237, China; [orcid.org/0000-0002-5244-870X](https://orcid.org/0000-0002-5244-870X); Email: lishengying@sdu.edu.cn

### Authors

**Tianjian Sun** – State Key Laboratory of Microbial Technology, Shandong University, Qingdao, Shandong 266237, China

**Mingyu Liu** – State Key Laboratory of Microbial Technology, Shandong University, Qingdao, Shandong 266237, China; Laboratory for Marine Biology and Biotechnology, Qingdao Marine Science and Technology Center, Qingdao, Shandong 266237, China; [orcid.org/0000-0001-8096-486X](https://orcid.org/0000-0001-8096-486X)

**Shuai Li** – State Key Laboratory of Microbial Technology, Shandong University, Qingdao, Shandong 266237, China

**Jiawei Guo** – State Key Laboratory of Microbial Technology, Shandong University, Qingdao, Shandong 266237, China

**Lei Liu** – School of Chemistry and Chemical Engineering, Shandong University, Jinan, Shandong 250100, China; [orcid.org/0000-0002-0839-373X](https://orcid.org/0000-0002-0839-373X)

**Lixin Zhang** – State Key Laboratory of Bioreactor Engineering, and School of Biotechnology, East China University of Science and Technology, Shanghai 200237, China

Complete contact information is available at: <https://pubs.acs.org/doi/10.1021/acscatal.4c06900>

### Author Contributions

<sup>#</sup>T.S. and M.L. contributed equally to this work.

### Notes

The authors declare no competing financial interest.

## ■ ACKNOWLEDGMENTS

This work was supported by the National Natural Science Foundation of China (32025001, 32071266, and 31600045) and the Natural Science Foundation of Shandong Province (ZR2019ZD20). We thank Prof. Yaojun Tong at Shanghai Jiao Tong University for providing us with the CRISPR-cBEST plasmid. We also thank Guannan Lin, Jingyao Qu, and Haiyan Sui from the State Key laboratory of Microbial Technology at Shandong University for their assistance in HPLC-HRMS and NMR spectroscopy analyses.

## REFERENCES

- (1) Tang, M. C.; Zou, Y.; Watanabe, K.; Walsh, C. T.; Tang, Y. Oxidative Cyclization in Natural Product Biosynthesis. *Chem. Rev.* **2017**, *117* (8), 5226–5333.
- (2) Lorente, A.; Lamariano-Merketegi, J.; Albericio, F.; Álvarez, M. Tetrahydrofuran-Containing Macrolides: A Fascinating Gift from the Deep Sea. *Chem. Rev.* **2013**, *113* (7), 4567–4610.
- (3) Fernández-Peña, L.; Díez-Poza, C.; González-Andrés, P.; Barbero, A. The Tetrahydrofuran Motif in Polyketide Marine Drugs. *Mar. Drugs* **2022**, *20* (2), 120.
- (4) Sachdeva, H.; Khaturia, S.; Saquib, M.; Khatik, N.; Khandelwal, A. R.; Meena, R.; Sharma, K. Oxygen- and Sulphur-Containing Heterocyclic Compounds as Potential Anticancer Agents. *Appl. Biochem. Biotechnol.* **2022**, *194* (12), 6438–6467.
- (5) Ikeda, H.; Omura, S. Avermectin Biosynthesis. *Chem. Rev.* **1997**, *97* (7), 2591–2610.
- (6) Burg, R. W.; Miller, B. M.; Baker, E. E.; Birnbaum, J.; Currie, S. A.; Hartman, R.; Kong, Y. L.; Monaghan, R. L.; Olson, G.; Putter, L.; Tunac, J. B.; Wallick, H.; Stapley, E. O.; Oiwa, R.; Omura, S. Avermectins, New Family of Potent Anthelmintic Agents: Producing Organism and Fermentation. *Antimicrob. Agents Chemother.* **1979**, *15* (3), 361–367.
- (7) Omura, S.; Crump, A. The Life and Times of Ivermectin - A Success Story. *Nat. Rev. Microbiol.* **2004**, *2* (12), 984–989.
- (8) Wolstenholme, A. J.; Rogers, A. T. Glutamate-Gated Chloride Channels and the Mode of Action of the Avermectin/Milbemycin Anthelmintics. *Parasitology* **2005**, *131* Suppl, S85–95.
- (9) Tambo, E.; Khater, E. I. M.; Chen, J. H.; Bergquist, R.; Zhou, X. N. Nobel Prize for the Artemisinin and Ivermectin Discoveries: A Great Boost towards Elimination of the Global Infectious Diseases of Poverty. *Infect. Dis. Poverty* **2015**, *4*, 58.
- (10) Taylor, M. J.; Hoerauf, A.; Bockarie, M. Lymphatic Filariasis and Onchocerciasis. *Lancet* **2010**, *376* (9747), 1175–1185.
- (11) Cane, D. E.; Liang, T. C.; Kaplan, L.; Nallin, M. K.; Schulman, M. D.; Hensens, O. D.; Douglas, A. W.; Albers-Schoenberg, G. Biosynthetic Origin of the Carbon Skeleton and Oxygen Atoms of the Avermectins. *J. Am. Chem. Soc.* **1983**, *105* (12), 4110–4112.
- (12) Ikeda, H.; Nonomiya, T.; Usami, M.; Ohta, T.; Omura, S. Organization of the Biosynthetic Gene Cluster for the Polyketide Anthelmintic Macrolide Avermectin in *Streptomyces avermitilis*. *Proc. Natl. Acad. Sci. U. S. A.* **1999**, *96* (17), 9509–9514.
- (13) Omura, S.; Ikeda, H.; Ishikawa, J.; Hanamoto, A.; Takahashi, C.; Shinose, M.; Takahashi, Y.; Horikawa, H.; Nakazawa, H.; Osonoe, T.; Kikuchi, H.; Shiba, T.; Sakaki, Y.; Hattori, M. Genome Sequence of an Industrial Microorganism *Streptomyces avermitilis*: Deducing the Ability of Producing Secondary Metabolites. *Proc. Natl. Acad. Sci. U. S. A.* **2001**, *98* (21), 12215–12220.
- (14) Sun, P.; Zhao, Q.; Yu, F.; Zhang, H.; Wu, Z.; Wang, Y.; Wang, Y.; Zhang, Q.; Liu, W. Spiroketal Formation and Modification in Avermectin Biosynthesis Involves a Dual Activity of AveC. *J. Am. Chem. Soc.* **2013**, *135* (4), 1540–1548.
- (15) Ikeda, H.; Takada, Y.; Pang, C. H.; Matsuzaki, K.; Tanaka, H.; Omura, S. Direct Production of 5-Oxo Derivatives of Avermectins by a Recombinant Strain of *Streptomyces avermitilis*. *J. Antibiot.* **1995**, *48* (1), 95–97.
- (16) Ikeda, H.; Wang, L. R.; Ohta, T.; Inokoshi, J.; Omura, S. Cloning of the Gene Encoding Avermectin B 5-O-Methyltransferase in Avermectin-Producing *Streptomyces avermitilis*. *Gene* **1998**, *206* (2), 175–180.
- (17) Hong, Y.-S.; Lee, J. H.; Kim, H. S.; Kim, K.-W.; Lee, J. J. Targeted Gene Disruption of the Avermectin B O-Methyltransferase Gene in *Streptomyces avermitilis*. *Biotechnol. Lett.* **2001**, *23* (21), 1765–1770.
- (18) MacNeil, D. J.; Gewain, K. M.; Ruby, C. L.; Dezeny, G.; Gibbons, P. H.; MacNeil, T. Analysis of *Streptomyces avermitilis* Genes Required for Avermectin Biosynthesis Utilizing a Novel Integration Vector. *Gene* **1992**, *111* (1), 61–68.
- (19) Zhang, C.; Albermann, C.; Fu, X.; Thorson, J. S. The in Vitro Characterization of the Iterative Avermectin Glycosyltransferase AveBI Reveals Reaction Reversibility and Sugar Nucleotide Flexibility. *J. Am. Chem. Soc.* **2006**, *128* (51), 16420–16421.
- (20) Pang, C. H.; Matsuzaki, K.; Ikeda, H.; Tanaka, H.; Omura, S. Production of 6,8a-Seco-6,8a-deoxy Derivatives of Avermectins by a Mutant Strain of *Streptomyces avermitilis*. *J. Antibiot.* **1995**, *48* (1), 59–66.
- (21) Tsou, H. R.; Ahmed, Z. H.; Fiala, R. R.; Bullock, M. W.; Carter, G. T.; Goodman, J. J.; Borders, D. B. Biosynthetic Origin of the Carbon Skeleton and Oxygen Atoms of the LL-F28249 Alpha, a Potent Antiparasitic Macrolide. *J. Antibiot.* **1989**, *42* (3), 398–406.
- (22) Chen, T. S.; Inamine, E. S. Studies on the Biosynthesis of Avermectins. *Arch. Biochem. Biophys.* **1989**, *270* (2), 521–525.
- (23) He, J.; Müller, M.; Hertweck, C. Formation of the aureothin Tetrahydrofuran Ring by a Bifunctional Cytochrome P450 Monooxygenase. *J. Am. Chem. Soc.* **2004**, *126* (51), 16742–16743.
- (24) Kwon, M.; Utomo, J. C.; Park, K.; Pascoe, C. A.; Chiorean, S.; Ngo, I.; Pelot, K. A.; Pan, C.-H.; Kim, S.-W.; Zerbe, P.; Vederas, J. C.; Ro, D.-K. Cytochrome P450-Catalyzed Biosynthesis of a Dihydrofuran Neoclerodane in Magic Mint (*Salvia divinorum*). *ACS Catal.* **2022**, *12* (1), 777–782.
- (25) Rudolf, J. D.; Dong, L. B.; Manogian, K.; Shen, B. Biosynthetic Origin of the Ether Ring in Platensimycin. *J. Am. Chem. Soc.* **2016**, *138* (51), 16711–16721.
- (26) Gao, Q.; Tan, G.-Y.; Xia, X.; Zhang, L. Learn from Microbial Intelligence for Avermectins Overproduction. *Curr. Opin. Biotechnol.* **2017**, *48*, 251–257.
- (27) Tong, Y.; Whitford, C. M.; Robertsen, H. L.; Blin, K.; Jørgensen, T. S.; Klitgaard, A. K.; Gren, T.; Jiang, X.; Weber, T.; Lee, S. Y. Highly Efficient DSB-Free Base Editing for Streptomyces with CRISPR-BEST. *Proc. Natl. Acad. Sci. U. S. A.* **2019**, *116* (41), 20366–20375.
- (28) de Marco, A. Strategies for Successful Recombinant Expression of Disulfide Bond-Dependent Proteins in *Escherichia coli*. *Microb. Cell Fact.* **2009**, *8*, 26.
- (29) Abramson, J.; Adler, J.; Dunger, J.; Evans, R.; Green, T.; Pritzel, A.; Ronneberger, O.; Willmore, L.; Ballard, A. J.; Bambrick, J.; Bodenstein, S. W.; Evans, D. A.; Hung, C.-C.; O'Neill, M.; Reiman, D.; Tunyasuvunakool, K.; Wu, Z.; Žemgulytė, A.; Arvaniti, E.; Beattie, C.; Bertolli, O.; Bridgland, A.; Cherepanov, A.; Congreve, M.; Cowen-Rivers, A. I.; Cowie, A.; Figurnov, M.; Fuchs, F. B.; Gladman, H.; Jain, R.; Khan, Y. A.; Low, C. M. R.; Perlin, K.; Potapenko, A.; Savy, P.; Singh, S.; Stecula, A.; Thillaisundaram, A.; Tong, C.; Yakneen, S.; Zhong, E. D.; Zielinski, M.; Židek, A.; Bapst, V.; Kohli, P.; Jaderberg, M.; Hassabis, D.; Jumper, J. M. Accurate Structure Prediction of Biomolecular Interactions with AlphaFold 3. *Nature* **2024**, *630* (8016), 493–500.
- (30) Esposito, D.; Chatterjee, D. K. Enhancement of Soluble Protein Expression through the Use of Fusion Tags. *Curr. Opin. Biotechnol.* **2006**, *17* (4), 353–358.
- (31) Saibil, H. Chaperone Machines for Protein Folding, Unfolding and Disaggregation. *Nat. Rev. Mol. Cell Biol.* **2013**, *14* (10), 630–642.
- (32) He, Y.; Sun, Y.; Liu, T.; Zhou, X.; Bai, L.; Deng, Z. Cloning of Separate Meilingmycin Biosynthesis Gene Clusters by Use of Acyltransferase-Ketoreductase Didomain PCR Amplification. *Appl. Environ. Microbiol.* **2010**, *76* (10), 3283–3292.
- (33) Omura, T.; Sato, R. The Carbon Monoxide-Binding Pigment of Liver Microsomes. II. Solubilization, Purification, and Properties. *J. Biol. Chem.* **1964**, *239*, 2379–2385.
- (34) Ogura, H.; Nishida, C. R.; Hoch, U. R.; Perera, R.; Dawson, J. H.; Ortiz de Montellano, P. R. EpoK, a Cytochrome P450 Involved in Biosynthesis of the Anticancer Agents Epothilones A and B. Substrate-Mediated Rescue of a P450 Enzyme. *Biochemistry* **2004**, *43* (46), 14712–14721.
- (35) Sun, Y. H.; Zeng, W. Q.; Benabbas, A.; Ye, X.; Denisov, I.; Sligar, S. G.; Du, J.; Dawson, J. H.; Champion, P. M. Investigations of Heme Ligation and Ligand Switching in Cytochromes P450 and P420. *Biochemistry* **2013**, *52* (34), 5941–5951.
- (36) Perera, R.; Sono, M.; Sigman, J. A.; Pfister, T. D.; Lu, Y.; Dawson, J. H. Neutral Thiol as a Proximal Ligand to Ferrous Heme

Iron: Implications for Heme Proteins that Lose Cysteine Thiolate Ligation on Reduction. *Proc. Natl. Acad. Sci. U.S.A.* **2003**, *100* (7), 3641–3646.

(37) Li, S.; Du, L.; Bernhardt, R. Redox Partners: Function Modulators of Bacterial P450 Enzymes. *Trends Microbiol.* **2020**, *28* (6), 445–454.

(38) Hannemann, F.; Bichet, A.; Ewen, K. M.; Bernhardt, R. Cytochrome P450 Systems—Biological Variations of Electron Transport Chains. *Biochim. Biophys. Acta* **2007**, *1770* (3), 330–344.

(39) Liu, X.; Li, F.; Sun, T.; Guo, J.; Zhang, X.; Zheng, X.; Du, L.; Zhang, W.; Ma, L.; Li, S. Three Pairs of Surrogate Redox Partners Comparison for Class I Cytochrome P450 Enzyme Activity Reconstitution. *Commun. Biol.* **2022**, *5* (1), 791.

(40) Zhang, W.; Du, L.; Li, F.; Zhang, X.; Qu, Z.; Han, L.; Li, Z.; Sun, J.; Qi, F.; Yao, Q.; Sun, Y.; Geng, C.; Li, S. Mechanistic Insights into Interactions between Bacterial Class I P450 Enzymes and Redox Partners. *ACS Catal.* **2018**, *8* (11), 9992–10003.

(41) Weckbecker, A.; Hummel, W. Glucose Dehydrogenase for The Regeneration of NADPH and NADH. In *Microbial Enzymes and Biotransformations*; Barredo, J. L., Ed.; Humana Press: Totowa, NJ, 2005; pp 225–238.

(42) Wang, Z. X.; Ravi Kumar, N.; Srivastava, D. K. A Novel Spectroscopic Titration Method for Determining the Dissociation Constant and Stoichiometry of Protein-Ligand Complex. *Anal. Biochem.* **1992**, *206* (2), 376–381.

(43) Meng, S.; Tang, G. L.; Pan, H. X. Enzymatic Formation of Oxygen-Containing Heterocycles in Natural Product Biosynthesis. *ChemBioChem.* **2018**, *19* (19), 2002–2022.

(44) Zhang, X.; Guo, J.; Cheng, F.; Li, S. Cytochrome P450 Enzymes in Fungal Natural Product Biosynthesis. *Nat. Prod. Rep.* **2021**, *38* (6), 1072–1099.

(45) Zhang, X.; Li, S. Expansion of Chemical Space for Natural Products by Uncommon P450 Reactions. *Nat. Prod. Rep.* **2017**, *34* (9), 1061–1089.

(46) Durairaj, P.; Li, S. Functional Expression and Regulation of Eukaryotic Cytochrome P450 Enzymes in Surrogate Microbial Cell Factories. *Eng. Microbiol.* **2022**, *2*, 100011.

(47) Li, Z.; Jiang, Y.; Zhang, X.; Chang, Y.; Li, S.; Zhang, X.; Zheng, S.; Geng, C.; Men, P.; Ma, L.; Yang, Y.; Gao, Z.; Tang, Y.-J.; Li, S. Fragrant Venezuelaenes A and B with a 5–5–6–7 Tetracyclic Skeleton: Discovery, Biosynthesis, and Mechanisms of Central Catalysts. *ACS Catal.* **2020**, *10* (10), 5846–5851.

(48) Li, Z.; Zhang, L.; Xu, K.; Jiang, Y.; Du, J.; Zhang, X.; Meng, L. H.; Wu, Q.; Du, L.; Li, X.; Hu, Y.; Xie, Z.; Jiang, X.; Tang, Y. J.; Wu, R.; Guo, R. T.; Li, S. Molecular Insights into the Catalytic Promiscuity of a Bacterial Diterpene Synthase. *Nat. Commun.* **2023**, *14* (1), 4001.

(49) Anzai, Y.; Li, S. Y.; Chaulagain, M. R.; Kinoshita, K.; Kato, F.; Montgomery, J.; Sherman, D. H. Functional Analysis of MycCI and MycG, Cytochrome P450 Enzymes Involved in Biosynthesis of Mycinamicin Macrolide Antibiotics. *Chem. Biol.* **2008**, *15* (9), 950–959.

(50) Crowe, J.; Döbeli, H.; Gentz, R.; Hochuli, E.; Stüber, D.; Henco, K. 6xHis-Ni-NTA Chromatography as a Superior Technique in Recombinant Protein Expression/Purification. *Methods Mol. Biol.* **1994**, *31*, 371–387.